Subscripto multiplex: A Riemannian symmetric positive definite strategy for offline signature verification

Elias N. Zois, Salem Said, Dimitrios Tsourounis, Alex Alexandridis

Subscripto multiplex: a Riemannian symmetric positive definite strategy for offline signature verification

Elias N. Zois[a*], **Salem Said**[b], **Dimitrios Tsourounis**[c], and **Alex Alexandridis**[a]

[a] Telsip Laboratory, University of West Attica, Petrou Ralli 250 Ave. Egaleo, 12241, Greece., Email: ezois@uniwa.gr , alexx@uniwa.gr

[b] CNRS, laboratoire LJK, Université Grenoble-Alpes, France. Email: salem.said@univ-grenoble-alpes.fr

[c] Department of Physics, University of Patras, Rio, 26504, Greece. Email: dtsourounis@upatras.gr

ABSTRACT: The human handwritten signature is considered to be a significant biometric trait. In the case of offline signatures, the problem is addressed as an image recognition task. On the other hand, the visual representation of symmetric positive definitive matrices, usually by means of the covariance descriptor of the image feature maps, forms a specific Riemannian manifold with a widespread usage and a favorable performance in a plethora of applications. Surprisingly, no records of offline-signature-verification-oriented research in the space of symmetric positive definitive matrix have been found up to now. In this work, we propose, for the first time in offline signature-verification literature, mapping of handwritten signature images in points of the tangent space of a connected symmetric positive definitive manifold for verification purposes. Furthermore, based on the principles of differential geometry, we address the notorious limited training problem of offline signature verification in this manifold by proposing two different feature augmentation methods. The efficiency of the proposed method is evaluated using three popular datasets of Western and Asian origin. Error rates against skilled and random forgery in both baselines as well augmentation scenarios are strong indicators of the informative and highly discriminative nature of symmetric positive definitive manifold oriented representation.

*Corresponding author. Tel.: +30-210-538-1559; fax: +30-210-538-7204; e-mail: ezois@uniwa.gr.

Can be also accessed via DOI: 10.1016/j.patrec.2023.02.002

1. Introduction

The authentication of the consent or presence of a human, by means of the signature, has been, an intriguing biometric authentication problem [1]. No need to say that signature-verification (SV) oriented research either online (or dynamic) or offline (or static) has considerable advancements. This is mainly due to the following four major facts: a) handwritten signatures like other behavioral traits cannot be forgotten, lost or stolen, b) signatures, contrary to other physiological biometric traits, have a natural variability, defined hereafter as intra-class variability which is the crucial factor for efficient verification, c) signatures are accepted as a social interface in a number of different types of societies as a trusted and non-invasive way to declare his/hers identity and d) it allows the fusion of several other scientific areas given the fact that the handwritten signature is an outcome of a cognitive task.

Review papers and surveys in SV [1-4], commonly categorize the methods as either dynamic-online (i.e. signal vs. time) [5-7] or static-offline (i.e. image) [8-13]. An alternative classification of offline signature verification methodologies divides them into a) handcrafted methods, which mainly utilize image processing and computer vision techniques and b) data-driven or learning-based approaches with typical representatives Bags of Visual Words [14, 15] sparse representation [11] and deep learning methodologies [8,12, 16-26]. The latter, address the problem by utilizing either classification [19, 27, 28] or metric learning [20, 21, 29] losses trained only with genuine samples [20, 30], or even along with skilled forgeries [12, 29]. The resulting network is contained within the feature extraction stage providing a vectored representation for any new test signature image [12, 19, 31, 32]. A number of deep learning based topologies are obtained by examining different loss functions [31] and similarity strategies [8,10, 30] commonly used on the dominant SigNet architecture. Also, post feature management methods are applied, exploiting the effectiveness of the extracted vectors [13, 33].

Another categorization differentiates them into Writer Dependent (WD) or Writer Independent (WI) according to the verification strategy that is followed [33-35]. In the WD approach a dedicated classifier is trained for each signatory with his/her reference samples [36-37]. They can perform efficiently with few reference samples, especially when synthetic signature samples are used [13, 38, 39]. The WI approach usually learns one global classifier which attempts to model the probability distribution between a) the intra-class of genuine-genuine pairs of signatures and b) the inter-class of genuine-forgery pairs by forming a (dis)similarity distance space [33, 35, 40, 41]. Deep learning based methods such as Attention Siamese networks [25] and Static-Dynamic Interaction Networks [26] have been also proposed.

The objective of offline signature verification methods is to provide a compact representation that efficiently captures the significant properties of the handwritten image. Such a representation should rely on a number of criteria like: (i) ability to uniquely characterize the signature contents, (ii) robustness under any potential deformations, affine or not, and (iii) stability and tolerance to occlusions. Simple descriptors such as normalized histograms of global or local patches of an image have been reported to partially fulfil criteria (i)-(iii). It is well known that one may advance any simple descriptor by appending additional image statistics such as edge orientations. Nevertheless, this idea comes with a cost; the existence of high-dimensional descriptors. An effective representation that integrates such multi-modal layers of information at a low dimensionality cost was introduced in [42], with the notion of the region covariance descriptors. The idea was to model a local part of the image using associations among different low-level layers of information. To this end, region covariance matrices are examples of symmetric positive definitive (SPD) matrix-based visual representations with favorable performance in a plethora of computer vision applications [43-46]. Remarkably, literature search shows that, to the author's best knowledge, no prior work has been presented which models the handwritten signature with the use of symmetric positive definitive matrices. Inspired by their use in visual representation, we introduce them in offline signature verification literature. The concept is relatively simple, since we compute new image planes such as intensity gradients, etc. and then we stack these raw features and compute their global (i.e. on the entire image) covariance matrix, resulting in the covariance descriptor. Below are the novelty characteristics of the proposed approach:

1. We propose for the first time, in the offline signature verification literature, a visual mapping of the signature image by measuring non-linear relations between pixel locations and values with the corresponding feature covariance matrix. This kind of non-Euclidean mapping maps a handwritten signature image into a point that relies on a special type of Riemannian homogenous space, namely, the symmetric positive definitive manifold. As a result, the concepts and algorithms of differential geometry can now be applied since covariance matrices are more naturally viewed through postulates and applications of curved geometry. This is important because, quite often, machine learning algorithms assumes that the input data forms vectors in Euclidean space. But what if the input data is immersed into a non-Euclidean space? Ignoring this geometrical constraint on the intrinsic structure of data may provide suboptimal results. It is worth noting here that we incorporate the geometry of the space by working with data sampled from a manifold whose geometry is well known, and do not pursue to learn the structure of the manifold as in manifold-learning procedures.

2. In order to address the notorious limited training data curse of pattern recognition, especially in offline signature verification [13, 24] we propose two methods for feature points augmentation or duplicates. To be specific, we propose two methods for the creation of duplicate covariance matrices when only a few (e.g. three) genuine reference covariance matrices - points are available for training. The first approach utilizes the notion of the geodesic curve between signature samples [47] for the creation of duplicates. The second one, uses fixed Riemannian Gaussian Distributions (RGD) on the space of symmetric positive definitive matrices [48, 49] with their maximum likelihood estimators evaluated from the samples of the learning population.

In this work, section 2 provides the mathematical tools of the Riemannian manifold of SPD matrices. Section 3 summarizes the concept of the global covariance matrix and describes the way in which they are used for modelling the handwritten signature images. Section 4 provides two mathematical models for creating duplicates in the manifold. Section 5 describes the experimental methods and results. Finally, section 6 provides the conclusion.

2. The Riemannian manifold of SPD matrices.

From this point on, unless otherwise specified, bold lowercase letters (e.g. $\mathbf{x}$) denote symmetric matrices, while bold capital letters (e.g. $\mathbf{X}$) denote SPD matrices. Small lowercase letters (e.g. $\mathbf{z}_{i,j}$ or $\mathbf{Z}_{i,j}$) denote the (i, j) elements of a matrix, lowercase or capital. In computer vision we often encounter mathematical entities that do not form Euclidean spaces but instead lie on nonlinear manifolds. Among the most popular examples are a) the space of linear subspaces of a Euclidean space formally known as the Grassman manifold and b) the space of SPD matrices. Following [50], we define a topological manifold (or simply manifold) as a topological space that is locally homomorphic to the *n*-dimensional Euclidean space $\mathbb{R}^n$. A differentiable manifold is a manifold that has a globally defined differential structure. This allows us to define derivatives (velocities) of curves on the manifold. The derivatives at any point $\mathbf{X}$ on the manifold lie in a vector space Tx which is expressed by symmetric matrices. The Tx is the tangent space of the $\mathbf{X}$ point (or pole) which provides all possible curves that pass through it.

A Riemannian manifold M is defined as a differentiable manifold with a smoothly varying inner product $\langle , \rangle_{\mathbf{X} \in M}$ on each point and corresponding tangent space [51]. In other words, we say that the Riemannian manifold is equipped with a corresponding Riemannian metric or norm of a tangent vector $\mathbf{y} \in \mathbf{T}_{\mathbf{X}}$ such that $\|y\|_{\mathbf{X}}^2 = \langle \mathbf{y} | \mathbf{y} \rangle_{\mathbf{X}}$. This allows us to define a number of useful geometric properties on the manifold such as (a) the angle between two curves passing through a point and (b) the length of a curve connecting two points. The shortest curve connecting two points $\mathbf{X}$ and $\mathbf{Y}$ is always a geodesic curve (a curve of zero acceleration). Its length defines the corresponding geodesic distance $d(\mathbf{X}, \mathbf{Y})$ and intuitively, geodesics is analogous to straight lines in $\mathbb{R}^n$. Given a point $\mathbf{X} \in M$ and a tangent vector $\mathbf{y} \in T_{\mathbf{X}}$, a unique geodesic curve $\mathbf{\Gamma}(t)$ exists such as $\mathbf{\Gamma}(0) = \mathbf{X}$ and its time derivative $\dot{\mathbf{\Gamma}}(t) = \mathbf{y}$. The Riemannian exponential map $exp_{\mathbf{X}} : T_{\mathbf{x}} \to M$ is defined by $exp_{\mathbf{X}}(\mathbf{y}) = \mathbf{\Gamma}(1)$. In the following, we only consider Riemannian manifolds which verify the identity $d(\mathbf{X}, exp_{\mathbf{X}}(\mathbf{y})) = \|\mathbf{y}\|_{\mathbf{X}}$ and which have a well-defined logarithm map:

$log_{\mathbf{X}} = exp_{\mathbf{X}}^{-1} : M \to T_{\mathbf{X}}$. In this case, it follows that $d(\mathbf{X},\mathbf{Y}) = \|\log_{\mathbf{X}}(Y)\|_{\mathbf{X}}$ and therefore a closed-form expression for the distance between points $\mathbf{X}$ and $\mathbf{Y}$ exists.

2.1. The Riemannian SPD manifold

Let $M \triangleq P_n$ denote the space P_n of all $n \times n$ real matrices Z which are symmetric and strictly positive definite: $\mathbf{Z}^T - \mathbf{Z} = \mathbf{0}$ and $v^T \mathbf{Z} v > \mathbf{0}$, for all $v \in \mathbb{R}^n$. This section considers the Riemannian geometry of the space P_n when it is equipped with the Rao-Fisher metric [52], defined by the inner products $\langle \mathbf{x} | \mathbf{y} \rangle_{\mathbf{X}} = tr[\mathbf{Y}^{-1}\mathbf{x}\mathbf{Y}^{-1}\mathbf{y}]^2$ for $\mathbf{x},\mathbf{y} \in \mathbf{T}_{\mathbf{X}}$, where tr. denotes the trace of a matrix. For this metric, the geodesic $\mathbf{\Gamma}(t)$ connecting two points $\mathbf{X}$ and $\mathbf{Y}$ is given by the one-valued parametric curve:

$$\mathbf{\Gamma}(t) = \mathbf{X}^{1/2}(\mathbf{X}^{-1/2}\mathbf{Y}\mathbf{X}^{-1/2})^t \mathbf{X}^{1/2}, \; t \in [0,1] \qquad (1)$$

so that $\mathbf{\Gamma}(0) = \mathbf{X}$ and $\mathbf{\Gamma}(1) = \mathbf{Y}$. This directly implies the Riemannian exponential and logarithm maps:

$$\mathbf{Y} \equiv exp_{\mathbf{X}}(\mathbf{y}) = \mathbf{X}^{1/2} exp(\mathbf{X}^{-1/2}\mathbf{y}\mathbf{X}^{-1/2})\mathbf{X}^{1/2} \qquad (2)$$

$$\mathbf{y} \equiv \log_{\mathbf{X}}(\mathbf{Y}) = \mathbf{X}^{1/2} log(\mathbf{X}^{-1/2}\mathbf{Y}\mathbf{X}^{-1/2})\mathbf{X}^{1/2} \qquad (3)$$

as well as the geodesic distance, called Rao's distance:

$$d^2(\mathbf{X},\mathbf{Y}) = tr[log(\mathbf{Y}^{-1/2}\mathbf{X}\mathbf{Y}^{1/2})]^2 = \sum_{i=1}^{n} log^2(\lambda_i) \qquad (4)$$

where λ_i are the eigenvalues of $\mathbf{Y}^{-1/2}\mathbf{X}\mathbf{Y}^{1/2}$. All matrix functions appearing in $\mathbf{\Gamma}(t)$ and eqs. (1-3) should be treated as symmetric matrix functions [53]. The Rao-Fisher metric turns the space P_n into a Riemannian homogeneous space under the action of the linear Group GL(n) of $n \times n$ real invertible matrices. This means that for any $\mathbf{X},\mathbf{Y} \in P_n$ here is a matrix $\mathbf{A} \in GL(n)$ which acts on $\mathbf{X} \in P_n$ by a congruence transformation $(\cdot)$ defined as: $(\mathbf{X},\mathbf{A}) \to \mathbf{X} \cdot \mathbf{A}$, $\mathbf{X} \cdot \mathbf{A} = \mathbf{A}^T \mathbf{X} \mathbf{A}$ in such a way that $\mathbf{X} \cdot \mathbf{A} = \mathbf{Y}$. In addition, the Rao-Fisher metric remains invariant under the action of GL(n) on P_n [49]. Figure 1, presents a graphical illustration of the aforementioned topics and at the same time provides a description of the proposed method. Any signature image I is modelled with one SPD matrix $\mathbf{Y}$ (i.e. a point at the P_n manifold). Next, the $\mathbf{Y}$ matrix is mapped on the tangent plane of a common pole $\mathbf{I}_{n\times n}$. This creates the tangent vector **y**with respect to a common tangential origin $\mathbf{0}_{n\times n} = \log_{\mathbf{I}_{n\times n}}(\mathbf{I}_{n\times n})$. Finally, the feature vector arises by evaluating the orthonormal coordinates of the tangent vector **y** in the $\mathbf{I}_{n\times n}$ common pole tangent space by a) applying the vector operator $vec_{\mathbf{I}_{9\times 9}}(\mathbf{y})$ as: $\mathbf{v} = vec_{\mathbf{I}_{n\times n}}(\mathbf{y}) = (\mathbf{I}_{n\times n}^{-1/2}\mathbf{y}\mathbf{I}_{n\times n}^{-1/2})$ and b) selecting its n(n+1)/2 components according to: $[\mathbf{v}_{1,1}, \sqrt{2}\mathbf{v}_{1,2}, ..., \mathbf{v}_{2,2}, \sqrt{2}\mathbf{v}_{2,3}, .., \mathbf{v}_{n,n}]$.

3. Covariance descriptors for offline SV

Let $I \in \mathbb{R}^{w\times h}$ be a gray scale or binary image of w-columns and h-rows and $F \in \mathbb{R}^{w\times h\times n}$ be a corresponding feature map stack with n raw image planes, evaluated from I with the use of a number of filters: $F(x,y) = \Phi(I,x,y)$. The function Φ can be any type of a series of mappings such as intensity, gradients, pixel locations, filter mappings, etc. Given a rectangular region $\mathfrak{R} \subset F$, let $\mathbf{f} = \{\mathbf{f}_i\}_{i=1,2,..,S} \in \mathbb{R}^{n\times S}$, be a local feature map of S total pixels that reside on $\mathfrak{R}$. Then, the region $\mathfrak{R}$ is modelled by the covariance matrix $C_{\mathfrak{R}} \in \mathbb{R}^{n\times n}$ of the $\mathbf{f}_i \in \mathbb{R}^n$ points evaluated as:

$$C_{\mathfrak{R}} = \frac{1}{S-1}\sum_{i=1}^{S}(\mathbf{f}_i - \boldsymbol{\mu})(\mathbf{f}_i - \boldsymbol{\mu})^T \qquad (5)$$

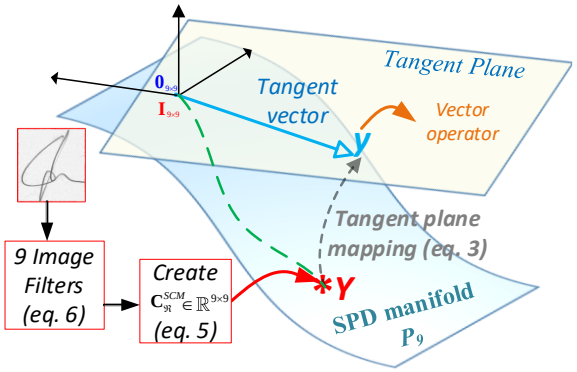

Fig. 1. *A signature image is represented by its corresponding CR matrix (one manifold point Y at the P9 SPD manifold). The logarithmic map computes the tangent vector y with respect to a common manifold pole* $\mathbf{I}_{n\times n}$ *and its corresponding origin* $\mathbf{0}_{n\times n}$ *of the tangent plane. Then, a vector operator is applied on the tangent vector y in order to have the final feature vector. The Green line represents the geodesic from the manifold origin* $\mathbf{I}_{n\times n}$ *to Y.*

where $\boldsymbol{\mu} \in \mathbb{R}^n$ represents the column mean vector of the $\mathbf{f}_i$ points and T denotes the transpose operator. This approach describes an accepted way for incorporating multiple types of features with potential correlation among them. It has been reported that $C_{\mathfrak{R}}$ is a powerful matching descriptor in scenarios which contain scenes with the object of interest, even in cases that the object is deformed in different views and poses [54]. The $C_{\mathfrak{R}}$ has a noise removal attribute due to the average filtering during its computation. In addition, $C_{\mathfrak{R}}$ does not have any explicit information regarding the position of pixels, which implies an inherent scale and rotation invariance over the region under examination. An appealing property comes from the fact that $C_{\mathfrak{R}}$ is considered to be low dimensional; it has only $n(n+1)/2$ different values. For every image under examination, the preprocessing step can be found in [11] and includes typical image processing steps as: thresholding with Otsu's method and thinning. The pruning level of thinning utilizes an automated algorithm originally proposed in [11] which measures an average 5×5 differential patch density of the image with respect to the applied thinning level. Next, the median value of the individual pruning levels of each signature image that belongs to the training set is set as the selected pruning level for any further image processing in both training and testing stages.

3.1. Global covariance descriptor for offline SV

For the addressed offline SV problem we define the following mapping $\Phi(I_p, x, y)$ of an initial signature image $I(x, y)$ as:

$$[I_p, |I_{p,x}|, |I_{p,y}|, |I_{p,xx}|, |I_{p,yy}|, \sqrt{I_{p,x}^2 + I_{p,y}^2}, \tan^{-1}(I_{p,y}/I_{p,x}), x_n, y_n] \qquad (6)$$

in which, $I_p \equiv I_p(x, y)$ is the grayscale signature image after the preprocessing step, $|I_{p,x}|, |I_{p,y}|, |I_{p,xx}|, |I_{p,yy}|$ are the first and second derivatives of $I_p(x, y)$ in both image directions, x_n, y_n are the signature pixel coordinates, normalized by the maximum number of rows and lines of the image bounding box and $\tan^{-1}(I_{p,y}/I_{p,x})$ is the gradient direction, normalized into radians with range varying from [-π, π). The corresponding signature covariance matrix $C_{\mathfrak{R}}^{SCM}$ of any image is evaluated with eqs. (5-6) but under the constraint that only the pixels that are part of the signature trace of the preprocessing step contribute to the computation of $C_{\mathfrak{R}}^{SCM}$. Therefore, any signature image results in a $C_{\mathfrak{R}}^{SCM} \in \mathbb{R}^{9\times9}$ point ($C_{\mathfrak{R}}^{SCM} \in \mathrm{P}_9$) therefore inheriting an intrinsic dimensionality of $45 = 9(9+1)/2$. In the unlike case that $C_{\mathfrak{R}}^{SCM}$ is not strictly positive definite, it can be converted into an SPD matrix by adding a small regularization term $\lambda \mathbf{I}_{9x9}$ where λ has a small coefficient value set to 10^{-4} and $\mathbf{I}_{9\times9}$ is the identity

matrix [55]. Therefore the $C_{\Re}^{SCM}$ captures global characteristics of the signature image. The use of arbitrary-sized detection windows has not been addressed in this work for simplicity reasons and it is a subject of ongoing research. Figure 2 shows the construction of a $C_{\Re}^{SCM}$ for one handwritten signature image.

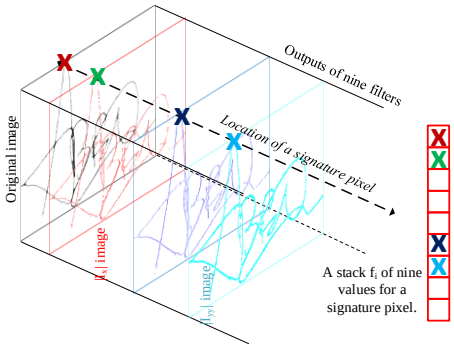

Fig. 2. *Creation of the* $C_{\Re}^{SCM}$ *: Original image and output of the filters. For a specific signature pixel marked with "x" in all filters-planes a column stack of values is created. Then, for all signature pixels, we compute its* $C_{\Re}^{SCM}$.

4. Creating duplicates in the SPD space

A challenging topic in Pattern Recognition and apparently in signature verification is to address the deficiency of available genuine reference samples for training as well as the need for training without any skilled forgeries [56]. This lack usually occurs due to the fact that, in a typical real-world acquisition scenario, persons do not undertake easily the task of creating several signature samples. In order to address this shortage, among others strategies, data augmentation algorithms have been introduced and reported more and more often, which provide synthetic signatures by duplicating real signature images [13, 57-59]. Another recent work [24] proposes a convolutional neural network model for offline HSV, called SigCNN, and utilize CycleGAN in style transfer fields to generate realistic offline signatures from online specimens and their duplicates. Also Maruyama et al. in [13] have proposed a duplicate feature generation process with notable results. Therefore it seems quite motivating to duplicate features instead of the signature itself. The improvement of the proposed SV duplication in terms of performance is associated with the way the duplicated signatures can model the intra and inter writer variability. This section proposes two methods for generating signature duplicates on the SPD space. The duplicates will be employed to augment the positive class of the training stage of the classifier in order to provide balanced populations between the positive and negative class populations.

4.1. Data augmentation on the geodesic curve

The parametric form of the geodesic curve $\mathbf{\Gamma}(t) \in P_n$ between two manifold points **X** and **Y** is given by eq. (1). Intuitively recall that the curve $\mathbf{\Gamma}(t) \in P_n$ is an infinite collection of manifold points in the geodesic defined with a one-dimensional parameter t. Therefore, given **X** and **Y** as the two ends of the geodesic curve we sample the $t \in [0,1]$ parameter of eq. (1) in order to create duplicate manifold points. In this work, two different variants of the parameter t are used. The first category, defined by the t_{GG} parameter, provides duplicate manifold points on the geodesic between two genuine reference samples. Therefore, we create duplicate points on the manifold that share common attributes between genuine reference samples on a path at the geodesic. In all experiments, the t_{GG} parameter was considered to be a random variable drawn from a uniform distribution $t_{GG} \sim U(0.2, 0.9)$. The second category, defined by the t_{GRF} parameter, provides duplicate SPD points on the geodesic between a reference sample and genuine samples of other writers, commonly known as random forgeries. Therefore we create SPD points that mimic the inter-variance of the genuine reference samples. In all our experiments, the t_{GRF} parameter takes one of two discrete relative small values $t_{GRF} \in \{0.05, 0.1\}$ and mimics the "genuine" side of the reference signatures. Figure 3, provides an illustration of the

geodesic-based duplicate method. Note that one could also provide duplicates between genuine duplicates and random forgeries etc.

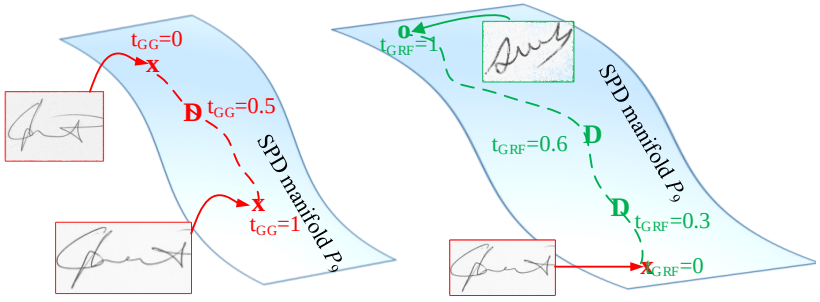

Fig. 3. *Illustration of the geodesic inspired duplicator. Red boxes, are genuine reference manifold points which are represented on the P_9 manifold with red 'x'. Green box is a random forgery, marked with green 'o'. (Left): geodesic curve between genuine samples along with duplicates (red 'D') by using the t_{GG} parameter. (Right): geodesic curve between genuine and random forgery samples along with duplicates (green 'D') by using the t_{GRF} parameter.*

4.2. Data augmentation with RGD's.

Given a number of few $C_{\Re}^{SCM}$ points on the SPD manifold (e.g. three) we create new duplicate points by utilizing the proposed Riemannian Gaussian distribution (RGD) parametric probabilistic model in the space of SPD matrices. In order to create SPD points with RGD's duplicates we follow the procedure below: First, we estimate the maximum likelihood estimate (MLE) of the RGD parameters with the set of few reference samples. Second, we build a symmetric positive definite RGD model with these parameters in order to draw the SPD duplicates. The proposed class of RGD probability model was formerly introduced by Pennec [48], explored in [60] and then expressed in an exact mathematical form in [49]. To begin, a symmetric positive definite RGD $\boldsymbol{C} \sim G\left(\bar{\boldsymbol{C}},\sigma\right)$ model is formally expressed with respect to the Riemannian volume element:

$$dv\left(\boldsymbol{C}\right) = \det\left(\boldsymbol{C}\right)^{-\frac{n+1}{2}} \prod_{i\le j} \boldsymbol{C}_{ij} \qquad (7)$$

where det(.) is the determinant, by the following probability density function:

$$p\left(\boldsymbol{C}|\bar{\boldsymbol{C}},\sigma\right) = \frac{1}{\zeta\left(\sigma\right)} exp\left[-\frac{d^2\left(\boldsymbol{C},\bar{\boldsymbol{C}}\right)}{2\sigma^2}\right] \qquad (8)$$

where $\bar{\boldsymbol{C}} \in P_n$ (in our case P_9), $\sigma \in \mathbb{R}_{>0}$ are the distribution parameters, $d\left(\boldsymbol{C},\bar{\boldsymbol{C}}\right)$ is Rao's distance and ζ(σ) is a normalizing factor. Note the resemblance of eq. (8) with the typical form of the one dimensional normal distribution. To continue, given a set of K-independent SPD points $\{\boldsymbol{C}_k\} = \{C_{\Re}^{SCM}\}_{i=1:k}$ drawn from $G(\bar{\boldsymbol{C}},\sigma)$, we estimate the empirical Riemannian center of mass $\boldsymbol{C}$ (of $\bar{\boldsymbol{C}}$) by evaluating the unique global minimizer of $\mathcal{E}_K : P_n \to \mathbb{R}_{\ge 0}$ [61]:

$$\mathcal{E}_K\left(\boldsymbol{C}\right) = \frac{1}{K}\sum_{k=1}^{K} d^2\left(\boldsymbol{C},\boldsymbol{C}_k\right) \qquad (9)$$

The existence and uniqueness of $\mathcal{E}_K$ holds from the proposition that if π is a probability distribution on P_n then π has a unique Riemannian center of mass $\bar{\boldsymbol{C}}_\pi$ which is a unique stationary point of the variance function $\mathcal{E}_\pi$ ([62], pp. 659). In our case, we set π to be the empirical distribution $\pi_K = (1/K)\left(\delta_{\boldsymbol{C}_1} + \delta_{\boldsymbol{C}_2} + \ldots + \delta_{\boldsymbol{C}_K}\right)$. Therefore, the solution $\hat{\sigma}_K$ of the following equation equals to the MLE $\hat{\sigma}_K$ of the parameter σ:

$$\sigma^3 \times \frac{d}{d\sigma} \log \zeta(\sigma) = \mathcal{E}_K\left(\hat{\boldsymbol{C}}_K\right) \tag{10}$$

Again, $\hat{\sigma}_K$ exists and is unique for any realization of the samples $\{\boldsymbol{C}_k\}$. Details regarding a smooth estimate of the solution of eq. (10) are provided in [63]. Given few samples from a reference set $\{\mathbf{C}_k\}$, the steps required to draw from a RGD are:

1. Compute the MLE $\hat{\boldsymbol{C}}_K$ (center of mass) of the $\{\boldsymbol{C}_k\}$ by solving eq. (9).

2. Compute the MLE of $\hat{\sigma}_K$ by solving eq. (10). For this purpose, the $\zeta(\sigma)$ normalizing factor has to be evaluated. In order to do so, polar coordinates have to be used for the representation of a SPD point $\boldsymbol{C}_k$ by means of its eigenvalues and eigenvectors. Specifically, for $r=(r_1,r_2,\ldots,r_n) \in \mathbb{R}^n$ and $U \in O(n)$, the group of n×n real orthogonal matrices we get from the spectral decomposition: $\mathbf{C}(r,U)=U^T \mathrm{diag}(e^r)U$. Due to the invariance property of the Riemannian homogeneous space, we have $\zeta(\sigma)=\zeta(\bar{\boldsymbol{C}},\sigma)=\zeta(\boldsymbol{I}_9,\sigma)$ and:

$$\begin{aligned}\zeta(\sigma) = \left(n!2^n\right)^{-1} \times \omega_n \times 8^{\frac{n(n-1)}{2}} \int_{\mathbb{R}^n} e^{-\left(\sum_i r_i^2\right)/2\sigma^2} \\ \times \prod_{i<j} sinh\left(\left|r_i - r_j\right|/2\right) \prod_{i=1}^{n} dr_i\end{aligned} \tag{11}$$

with $\omega_n = 2^n \pi^{n^2/2} / \Gamma_n(n/2)$, and Γ_n the multivariate gamma function. In P_9 the integral is numerically evaluated.

3. Compute and sample $r \in \mathbb{R}^n$ from the joint RGD density $p(r)$ with the Metropolis-Hastings algorithm.

$$\begin{aligned}p(r) = \left(n!2^n\right)^{-1} \times \omega_n \times 8^{\frac{n(n-1)}{2}} e^{-\left(\sum_i r_i^2\right)/2\sigma^2} \\ \times \zeta^{-1}(\sigma) \times \prod_{i<j} sinh\left(\left|r_i - r_j\right|/2\right)\end{aligned} \tag{12}$$

4. Sample from a uniform distribution on O(n). This is achieved by setting an n×n A matrix with independent entries from N(0,1) and if A=UT with U orthogonal and T triangular, then U is uniformly distributed on O(n).

5. From eq. (12) we obtain r and from step (4) we obtain U. Next, we use the spectral decomposition in order to synthesize and sample from $G(\mathbf{I},\sigma)$. Finally, due to the homogeneous property: expressed by $C \sim G(\bar{\boldsymbol{C}},\sigma) \Rightarrow \bar{\boldsymbol{C}} \cdot A \sim G(\bar{\boldsymbol{C}} \cdot \boldsymbol{A},\sigma)$, the sampling from Y~G(I,σ) is followed by $\boldsymbol{Y} \cdot \bar{\boldsymbol{C}}^{1/2}$ which in turn results to draw from a desired distribution $\boldsymbol{Y} \cdot \bar{\boldsymbol{C}}^{1/2} \sim G(\bar{\boldsymbol{C}},\sigma)$, centered on the empirical center of mass $\bar{\boldsymbol{C}} = \hat{\boldsymbol{C}}_K$ or alternatively on any reference SPD point $\boldsymbol{C}_k$, $\boldsymbol{Y} \cdot \boldsymbol{C}_k \sim G(\boldsymbol{C}_k,\sigma)$.

5. Methods and experimental results

Three offline handwritten signature datasets were used in order to evaluate the proposed SPD model. These are: the popular western oriented a) CEDAR [64] (24 genuine and forgery samples per user), the Indo-Aryan oriented: HINDI and BENGALI (24 genuine and 30 forgery samples per user), which are the two sub-sets of the BHSig260 database [65] [66]. Evaluation of any $C_{\Re}^{SCM}$ matrix considers only the locations and original values of those signature pixels that are part of the thinned signature.

Experiments were conducted under a writer depended (WD) framework and comply with mandatory protocols that appeared in classical and recent relevant papers [67, 68]. In all our experiments we designate with ${}^{(\text{duplicate method})}\omega^{L+}{}_{(\text{number of samples \& type})}$ and ${}^{(..)}\omega^{L-(..)}$ the positive and negative training classes which comprise a learning set L and by $\omega^{T+}{}_{(..)}$, $\omega^{T-}{}_{(..)}$ the positive and negative training classes of the testing set T. We performed a number of popular training scenarios. The first is referred hereafter as Baseline#1 (L_{BL1}) in which the learning set $L_{BL1}=[\omega^{L+}{}_{(10G)}, \omega^{L-}{}_{(50RF)}]$ represented by the proposed features, is formed by: a) setting the number of genuine (G) reference samples equal to $N_{GREF}=10$ for the positive class $\omega^{L+}{}_{(10G)} \in \mathbb{R}^{10\times 45}$ and b) setting the number of representatives of the negative class $\omega^{L-}{}_{(50RF)} \in \mathbb{R}^{50\times 45}$ to 50 random forgery (RF) samples provided by randomly selecting genuine samples from other writers of the respective dataset. The set L_{BL1} feeds a binary, radial basis support vector machine (SVM) classifier. In the testing stage, any questioned (Q) sample comes from one of the following categories: a) $\omega^{T+}{}_{(G)}$ as to represent the remaining genuine signatures, b) $\omega^{T-}{}_{(S)}$ as to represent the full set of the simulated or skilled (S) forgeries (i.e. 24 for CEDAR, 30 for Hindi and Bengali) or c) $\omega^{T-}{}_{(RF)}$ as to represent the remaining random forgeries of all the other writers of the dataset. We report the results by means of the average value (10 repetitions) of two corresponding Equal Error Rates (EER) with two user dependent sliding thresholds. The first is the EER(S), i.e. the probability of rejecting genuine samples p_{FRR} vs the probability of accepting skilled forgery samples $p_{FAR(S)}$, and the second is the EER(RF) i.e. the probability of rejecting genuine samples pFRR vs the probability of accepting random forgery samples $p_{FAR(RF)}$. It is important here to note that the testing stage does not contain the same RF samples of the Learning set. The second experimental setup referred hereafter as Baseline#2, (L_{BL2}) is similar to the LBL1, but it is more challenging since it has only three (3) genuine samples for the positive class $\omega^{L+}{}_{(3G)}$, and a number of 30 $\omega^{L-}{}_{(30RF)}$ samples for its negative class. This set is similar to the case in which a limited number of training samples are available. In an analogous way to the L_{BL1} design, same quality metrics and EER(S) and EER(RF) rates were measured and reported.

Next, we provide details for a number of experimental setups in which the positive class is comprised from a) the few training samples $\omega^{L+}{}_{(3G)}$ and b) their duplicates designated by $\omega^{L+}{}_{(Duplicate)}$ according to the material exposed in section 4. For the duplicate case provided in section 4.1 we now provide some additional clarifications. The fixed t_{GRF} parameter accepts two values: 0.1 and 0.01 in order to create genuine-random forgery duplicates $\omega^{L+}{}_{(D\text{-}GRF)}$. Pairing with 50 random forgeries of the $\omega^{L-}{}_{(50RF)}$ category, a total number of 3×50: $\omega^{L+}{}_{(150D\text{-}RF)}$ positive class duplicates are created and combined with the $\omega^{L-}{}_{(50RF)}$ negative class samples in order to create the first augmentation setup defined as L_{AUG1}. In addition to the sect. 4.1 discussion we construct another scenario in which we set $N_D^{GG}=5$, the number of genuine pair duplicates. The corresponding tGRF parameter draws N_D^{GG} times from a uniform distribution tGG~U(0.2, 0.9). Therefore a total of $\omega^{L+}{}_{(D\text{-}GG)}$ genuine to genuine (GG) duplicates is created. Consequently, GG to RF (GG-RF) duplicates can be created and appended to $\omega^{+}{}_{(Duplicate)}$ class by pairing the aforementioned $\omega^{L+}{}_{(D\text{-}GG)}$ samples and the $\omega^{-}{}_{(50RF)}$ negative class samples; the total number of duplicates then is equal to $\omega^{L+}{}_{(750D\text{-}GGRF)}$ duplicates. We denote this experimental setup as L_{AUG2}.

For the RGD duplicate case (section 4.2) we also provide a description of tasks. For any given population of the $\omega^{L+}{}_{(3G)}$ samples we solve eqs.(9,10) for evaluation of the dispersion parameter $\hat{\sigma}(\omega_{3G}^{L+})$ throughout the Karcher mean $\hat{\mathbf{C}}(\omega_{3G}^{L+})$. Then, using steps (1)-(5) of section 4.2 we create duplicates by direct RGD sampling from either: i) three individual RGD distributions $G\left(\boldsymbol{C}_i, \hat{\sigma}(\omega_{3G}^{L+})\right)$ in which each of the center Ci is one reference sample from the original $\omega^{L+}{}_{(3G)}$ set and ii) three RDG's G(Ci, σ_{fixed}) with σ_{fixed} equals to 0.1 or 0.01. To avoid any potential confusion we state here that the MLE $\hat{\mathbf{C}}$ is only used for evaluation of the MLE of $\hat{\sigma}$; therefore we did not choose to perform direct RGD sampling from the $G(\hat{\mathbf{C}}(\omega_{3G}^{L+}), \hat{\sigma}(\omega_{3G}^{L+}))$ distribution. The number of direct RGD sampling based duplicates was also set to five (5) which result in a corresponding ${}^{(RGD)}\omega^{L+}{}_{(15D\text{-}G)}$ number of positive set samples of a new L_{AUG3} set. Finally, in a similar way to L_{AUG2}, we can choose to append the ${}^{(RGD)}\omega^{L+}{}_{(15D\text{-}G)}$ set by pairing them with 50 random forgeries of the $\omega^{L-}{}_{(50RF)}$ negative class samples. A total of ${}^{(RGD)}\omega^{L+}{}_{(750D\text{-}GRF)}$ is created with the t_{GRF}

parameter, thus creating the positive class of the L_{AUG3} set. The number of samples ω^{L-} of the negative class has been set equal to the number of the positive class ω^{L+} by drawing additional random forgery samples only when ω^{L+} population class exceeds 50. Table 1 provides a summary of the proposed experimental setups.

Table 1. Summary of proposed experimental setups.

Setup	Case	Learning Set (+) class	Learning Set (-) class	Testing Set (+) & (-) classes
LBL1	-	$\omega^{L+}_{(10G)}$	$\omega^{L-}_{(50RF)}$	The ω^{T+}class contains the remaining genuine samples ω^{T+}(G) The ω^{T-} class contains: i) all the (S)killed forgery samples ω^{T-}(S) or ii) all the remaining (R)andom (F)orgery samples ω^{T-}(RF).
LBL2	-	$\omega^{L+}_{(3G)}$		
LAUG1	a	$\omega^{L+}_{(150D\text{-}RF)}$	$\omega^{L-}_{(150RF)}$	
	b	$\omega^{L+}_{(3G)}$ & $\omega^{+L}_{(150D\text{-}RF)}$	$\omega^{L-}_{(153RF)}$	
LAUG2	a	$\omega^{L+}_{(15D\text{-}GG)}$	$\omega^{L-}_{(50RF)}$	
	b	$\omega^{L+}_{(750D\text{-}GGRF)}$	$\omega^{L-}_{(750RF)}$	
	c	$\omega^{L+}_{(3G)}$ & $\omega^{L+}_{(750D\text{-}GGRF)}$	$\omega^{L-}_{(50RF)}$	
	d	$\omega^{L+}_{(3G)}$ & $\omega^{L+}_{(15D\text{-}GG)}$ & $\omega^{L+}_{(750D\text{-}GGRF)}$	$\omega^{L-}_{(768RF)}$	
LAUG3	a	$^{(RGD)}\omega^{L+}_{(15D\text{-}G)}$	$\omega^{L-}_{(50RF)}$	
	b	$\omega^{L+}_{(3G)}$ & $^{(RGD)}\omega^{L+}_{(15D\text{-}G)}$		
LAUG4	a	$^{(RGD)}\omega^{L+}_{(15D\text{-}G)}$	$\omega^{L-}_{(750RF)}$	
	b	$\omega^{L+}_{(3G)}$ & $^{(RGD)}\omega^{L+}_{(15D\text{-}G)}$	$\omega^{L-}_{(753RF)}$	

5.1. Results

The experiments were conducted 10 times and averages of user dependent EER's in both (S) and (RF) scenarios are shown in table 2. Commenting on the results, we primarily note the improved performance of the random forgery experiment when compared to the skilled forgery one, something that is a reasonable outcome. We also note the low verification error rates derived with the typical setups of the LBL1 with 10 reference samples as well as the limited training sample setup LBL2 with only three samples. Tables 3 and 4 provide the verification errors when covariance matrix augmentation actions are taking place. When we consider geodesic based duplicates we observe that the lowest verification error rates are derived when t_{GRF}=0.05 for the case of creating duplicates located on the geodesic between genuine reference samples and random forgeries. On the other hand, if we set t_{GRF}=0.1, a minor degradation in verification efficiency is observed. Similar issues are observed when RGD duplicates are also created. The weakest verification efficiency is obtained when the random forgeries do not participate in the formation of the duplicates and we estimate the parameter σ with $\hat{\sigma}(\omega_{3G}^{L+})$. On the other hand, low error rates are observed, when σ is estimated with $\hat{\sigma}(\omega_{3G}^{L+})$ and we utilize random forgeries by taking t_{GRF}=0.05 (with similar error rates observed when tGRF=0.1). In the case of manually setting σ, improved verification results are obtained when σ=0.01, with an additional minor improvement when random forgeries are participating in the creation of duplicates. This is a quite interesting result; one may observe from the joint RGD density (section 4.2, step 3) that r~p(r) provides the *exp*(*r*) term needed for the spectral decomposition (and synthesis) with values near 1, or near the volume of any $\mathbf{C}_k$ sample with the use of eq.(12). We know that the eigenvalues of a covariance matrix are representative of the hyper-ellipsoid volume that embeds the 9-dimensional signature pixels feature maps. So, this might be an indication that the improvement of the duplicate method is mainly due to the sampling from O(n) by means of the orthogonal matrix U which is uniformly distributed on O(n).

Table 2. Baseline error rates (EER(S) & EER(RF) %)

Baseline# & #Refs	EER(S) & EER(RF) user_thresholds CEDAR	HINDI	BENGALI
L_{BL1}(10G)	0.49(S) 0.03(RF)	1.00(S) 0.30 (RF)	0.27(S) 0.09(RF)
L_{BL2}(3G)	1.18(S) 0.14(RF)	2.50(S) 0.69 (RF)	1.52(S) 0.41 (RF)

A summary of some recent state-of-the-art (SOTA) results is shown in Tables 5 and 6 for both baselines and augmentation writer dependent setups. Table 5 contains direct comparisons (i.e. same experiments, same random seeds in the selection of genuine samples and RF's in the 10-fold repetition) with the methods that have been developed by the majority of the authors in other publications [9, 11]. We also provide a comparative summary with characteristic methods found in the literature given the fact that a more thorough comparison is not feasible given the numerous and diverse nature in the design and implementation of the system's stages. We additionally report here other augmentation research efforts i) the work of Yapici et al. [57] which utilized a novel cycle-GAN topology for generating synthetic signature images but did not evaluate the used datasets, ii) the work of Prajapati et al. [69] which exploited autoencoders for synthetic signatures; but it was restricted on a private Persian dataset and iii) the work of Ruiz et al. [58] tested only with random forgeries. We feel that that the proposed method is definitely worthy a new line of research for OSV.

Table 3. Error rates (EER(S) & EER(RF) %) for augmentation methods and duplicates placement on the geodesic curve.

Setup	Case	tGRF	CEDAR	HINDI	BENGALI
LAUG1	a	0.05	0.51(S) 0.12(RF)	1.65(S) 0.44(RF)	1.06(S) 0.32(RF)
		0.10	0.55(S) 0.13(RF)	1.65(S) 0.44(RF)	1.07(S) 0.32(RF)
	b	0.05	0.49(S) 0.12(RF)	1.62(S) 0.43(RF)	1.02(S) 0.31(RF)
		0.10	0.52(S) 0.12(RF)	1.61(S) 0.43(RF)	1.05(S) 0.32(RF)
LAUG2	a	0.05	0.67(S) 0.14(RF)	1.72(S) 0.54(RF)	1.27(S) 0.38(RF)
		0.10	0.73(S) 0.18(RF)	1.80(S) 0.60(RF)	1.24(S) 0.36(RF)
	b	0.05	0.49(S) 0.10(RF)	1.65(S) 0.46(RF)	0.99(S) 0.25(RF)
		0.10	0.51(S) 0.12(RF)	1.65(S) 0.45(RF)	0.99(S) 0.25(RF)
	c	0.05	0.64(S) 0.13(RF)	1.62(S) 0.45(RF)	1.21(S) 0.42(RF)
		0.10	0.70(S) 0.18(RF)	1.65(S) 0.45(RF)	1.18(S) 0.33(RF)
	d	0.05	0.45(S) 0.09(RF)	1.60(S) 0.43(RF)	0.90(S) 0.23(RF)
		0.10	0.47(S) 0.10(RF)	1.60(S) 0.43(RF)	0.95(S) 0.23(RF)

Table 4. Error rates (EER(S) & EER(RF) %) for augmentation methods and duplicates placement with RGD's.

RGD Parameters	**DATASET**		
	CEDAR	**HINDI**	**BENGALI**
		L_{AUG3} (Case a)	
G(**C**$_i$, $\hat{\sigma}(\omega_{3G}^{L+})$)	5.27(S) 2.42(RF)	13.9(S) 4.87(RF)	10.9(S) 3.41(RF)
G(**C**$_i$,0.01)	0.49(S) 0.12(RF)	1.67(S) 0.54(RF)	0.88(S) 0.23(RF)
G(**C**$_i$,0.1)	4.77(S) 2.21(RF)	11.2(S) 3.70(RF)	1.76(S) 0.55(RF)
		L_{AUG3} (Case b)	
G(**C**$_i$, $\hat{\sigma}(\omega_{3G}^{L+})$)	5.15(S) 2.28(RF)	13.0(S) 4.22(RF)	10.2(S) 3.24(RF)
G(**C**$_i$,0.01)	0.49(S) 0.10(RF)	1.60(S) 0.42(RF)	0.85(S) 0.22(RF)
G(**C**$_i$,0.1)	4.75(S) 2.18(RF)	12.1(S) 4.01(RF)	1.43(S) 0.40(RF)
		L_{AUG4} (Case a), tGRF=0.05	
G(**C**$_i$, $\hat{\sigma}(\omega_{3G}^{L+})$)	0.69(S) 0.14(RF)	1.72(S) 0.55(RF)	1.24(S) 0.41(RF)
G(**C**$_i$,0.01)	0.49(S) 0.11(RF)	1.60(S) 0.42(RF)	0.86(S) 0.22(RF)
G(**C**$_i$,0.1)	1.55(S) 0.16(RF)	1.89(S) 0.58(RF)	5.12(S) 1.76(RF)
		LAUG4 (Case b), tGRF=0.1	
G(**C**$_i$, $\hat{\sigma}(\omega_{3G}^{L+})$)	0.74(S) 0.15(RF)	1.82(S) 0.57(RF)	1.41(S) 0.53(RF)
G(**C**$_i$,0.01)	0.55(S) 0.11(RF)	1.62 (S) 0.45(RF)	0.92(S) 0.25(RF)
G(**C**$_i$,0.1)	1.73(S) 0.18(RF)	2.13(S) 0.63(RF)	5.22(S) 1.80(RF)

Table 5. Comparative summary of EER(S) % for WD baseline SOTA methods on skilled forgeries. The results reported on refs [11] and [9] are a direct comparison (i.e. same verification protocol) to the proposed.

Method(Ref)	CEDAR	HINDI	BENGALI
SigNet/F/SPP [12]	3.60(10G)	-	-
K-SVD/OMP [11]	0.79(10G)	1.05(10G)	0.44(10G)
Hybrid Texture [70]	1.64(16G)	10.9(16G): for all (260) writers	
RNN's [8]	0.01(12G)	0.43(12G)	0.36(12G)
Deformations [16]	3.89(12G)	9.01(8G)	8.21(8G)
Texture features [65]	-	24.4(8G)	33.8(8G)
CNN-CoLL [22]	2.50(3G)	-	-
Visibility Graphs [9]	0.51(10G)	1.02(10G)	0.32(10G)
Deep metric net [23]	1.67(12G)	-	-
Stroke aware GAN [24]	3.31(10G)	-	-
Proposed (LBL1)	0.49(10G)	1.00(10G)	0.27(10G)

Table 6. Comparative summary of error rates (EER%) for WD SOTA with some augmentation methods on skilled forgeries.

Method (Ref)	CEDAR	HINDI	BENGALI
Duplicator: [13, 71]	3.04(3G)[13]	-	6.06(5G)[71]
Gaussian noise: [13]	0.82(3G)	-	-
Stroke aware GAN [24]	5.65(3G)	-	-
Proposed (RGD's)	0.49(3G)	1.62(3G)	0.86(3G)

6. Conclusions

For the first time in offline SV we map signatures in the SPD manifold and in a common pole tangent space. Two new approaches are employed in order to cope with the limited training issue of SV in the view of the SPD manifold space. Experiments with a) a baseline setup, b) limited reference samples and c) the proposed duplicates were conducted in three popular datasets. Ongoing research includes the porting of the SPD manifold into the WI signature verification domain with more signature datasets that use different SPD metrics in order to propose a robust WI classifier.

References

1. M. Stauffer, P. Maergner, A. Fischer, K. Riesen, A Survey of State of the Art Methods Employed in the Offline Signature Verification Process, in: New Trends in Business Information Systems and Technology: Digit. Innovation and Digit. Bus. Transf., R. Dornberger, Ed., Springer, Cham, 2021, pp.17-30.
2. M. Diaz, M. A. Ferrer, D. Impedovo, M. I. Malik, G. Pirlo, R. Plamondon, A Perspective Analysis of Handwritten Signature Technology, ACM Comput. Surv. 51 (2019), doi: 0.1145/3274658.
3. D. Impedovo and G. Pirlo, Automatic Signature Verification: The State of the Art, IEEE Trans. Syst. Man, Cybern., Part C: 38,(2008) 609-635.
4. M. M. Hameed, R. Ahmad, M. L. M. Kiah, G. Murtaza, Machine learning-based offline signature verification systems: A systematic review, Signal Proc.: Image Communication, 93 (2021) 116139.
5. M. Faundez-Zanuy, J. Fierrez, M. A. Ferrer, M. Diaz, R. Tolosana, R. Plamondon, Handwriting Biometrics: Applications and Future Trends in e-Security and e-Health, Cognit. Comp., (12), 2020, 940-953.
6. J. Galbally, M. Diaz-Cabrera, M. A. Ferrer, M. Gomez-Barrero, A. Morales, and J. Fierrez, On-line signature recognition through the combination of real dynamic data and synthetically generated static data, Pattern Recognit. 48 (2015), 2921-2934.

7. N. Sae-Bae, N. Memon, and P. Sooraksa, Distinctiveness, complexity, and repeatability of online signature templates, Pattern Recognit., 84 (2018), 332-344.
8. R. Ghosh, A Recurrent Neural Network based deep learning model for offline signature verification and recognition system, Expert Syst. with Appl., 168 (2021), 114249, doi: 10.1016/j.eswa.2020.114249.
9. E. N. Zois, E. Zervas, D. Tsourounis, and G. Economou, Sequential Motif Profiles and Topological Plots for Offline Signature Verification, in Comput. Vis. Pattern Recognit., (CVPR) 2020, pp. 13245-13255.
10. M. B. Yılmaz and K. Öztürk, "Recurrent Binary Patterns and CNNs for Offline Signature Verification," Cham, 2020, pp. 417-434.
11. E. N. Zois, D. Tsourounis, I. Theodorakopoulos, A. L. Kesidis, G. Economou, A Comprehensive Study of Sparse Representation Techniques for Offline Signature Verification, IEEE Trans. Biom. Behav. Ident. Sc., 1 (2019), 68-81.
12. L. G. Hafemann, R. Sabourin, L. S. Oliveira, Learning features for offline handwritten signature verification using deep convolutional neural networks, Pattern Recognit., vol. 70, pp. 163-176, 2017.
13. T. M. Maruyama, L. S. Oliveira, A. S. Britto, R. Sabourin, Intrapersonal Parameter Optimization for Offline Handwritten Signature Augmentation, IEEE Trans. Inf. Forensics Secur. 16 (2021)1335-1350.
14. M. Okawa, Synergy of foreground–background images for feature extraction: Offline signature verification using Fisher vector with fused KAZE features, Pattern Recognit., 79 (2018), 480-489.
15. Y. Serdouk, H. Nemmour, Y. Chibani, Handwritten signature verification using the quad-tree histogram of templates and a Support Vector-based artificial immune classification, Image Vis. Comput. 66 (2017), 26-35.
16. Y. Zheng, B. K. Iwana, M. I. Malik, S. Ahmed, W. Ohyama, and S. Uchida, Learning the Micro Deformations by Max-pooling for Offline Signature Verification, Pattern Recognit., 118 (2021), 108008.
17. H. Li, P. Wei, P. Hu, AVN: An Adversarial Variation Network Model for Handwritten Signature Verification, IEEE Trans. Mult. 24 (2021) 594-608, doi: 10.1109/TMM.2021.3056217.
18. E. Parcham, M. Ilbeygi, M. Amini, CBCapsNet: A novel writer-independent offline signature verification model using a CNN-based architecture and capsule neural networks, Expert Syst. with Appl., 185 (2021), 115649.
19. D. Avola, M. J. Bigdello, L. Cinque, A. Fagioli, M. R. Marini, R-SigNet: Reduced Space Writer-Independent Feature Learning for Offline Writer-Dependent Signature Verification, Pattern Recognit. Lett, 150 (2021) 189-196.
20. P. Maergner, V. Pondenkandath, M. Alberti, M. Liwicki, K. Riesen, R. Ingold, A. Fischer, Combining graph edit distance and triplet networks for offline signature verification, Pattern Recognit. Lett., 125 (2019), 527-533.
21. Soleimani, B. N. Araabi, K. Fouladi, Deep Multitask Metric Learning for Offline Signature Verification, Pattern Recognit. Lett., 80 (2016), 84-90.
22. D. Tsourounis, I. Theodorakopoulos, E. N. Zois, G. Economou, From text to signatures: Knowledge transfer for efficient deep feature learning in offline signature verification, Expert Syst. with Appl., 189(2022) 116136.
23. L. Liu, L. Huang, F. Yin, Y. Chen, Offline signature verification using a region based deep metric learning network, Pattern Recognit., 118 (2021), 108009.
24. J. Jiang, S. Lai, L. Jin, Y. Zhu, J. Zhang, and B. Chen, Forgery-free signature verification with stroke-aware cycle-consistent generative adversarial network, Neurocomputing, 507 (2022),345-357.
25. Y.-J. Xiong and S.-Y. Cheng, Attention Based Multiple Siamese Network for Offline Signature Verification, Cham, 2021, pp. 337-349.
26. H. Li, P. Wei, and P. Hu, Static-Dynamic Interaction Networks for Offline Signature Verification, in: AAAI Conf. Artif. Intel., 2021, pp. 1893-1901.

27. L. G. Hafemann, R. Sabourin, and L. S. Oliveira, Analyzing features learned for Offline Signature Verification using Deep CNNs, in: Int. Conf. on Pattern Recognit. (ICPR), 2016.
28. Z. Zhang, X. Liu, and Y. Cui, Multi-phase Offline Signature Verification System Using Deep Convolutional Generative Adversarial Networks, in: Int. Symposium on Comput. Intel. Design (ISCID), 2016.
29. S. Dey, A. Dutta, J. I. Toledo, S. K. Ghosh, J. Lladós, and U. Pal, SigNet: Convolutional Siamese Network for Writer Independent Offline Signature Verification, arXiv preprint arXiv:1707.02131, 2017.
30. M. B. Yilmaz and K. Ozturk, Hybrid User-Independent and User-Dependent Offline Signature Verification With a Two-Channel CNN, in: IEEE Conf. (CVPRW), 2018.
31. S. Masoudnia, O. Mersa, B. N. Araabi, A.-H. Vahabie, M. A. Sadeghi, and M. N. Ahmadabadi, "Multi-Representational Learning for Offline Signature Verification using Multi-Loss Snapshot Ensemble of CNNs," Expert Systems with Applications, 2019/03/23/ 2019.
32. L. G. Hafemann, L. S. Oliveira, and R. Sabourin, "Fixed-sized representation learning from offline handwritten signatures of different sizes," International Journal on Document Analysis and Recognition (IJDAR), vol. 21, pp. 219-232, September 01 2018.
33. V. L. F. Souza, A. L. I. Oliveira, R. M. O. Cruz, and R. Sabourin, "A white-box analysis on the writer-independent dichotomy transformation applied to offline handwritten signature verification," Expert Systems with Applications, p. 113397, 2020/03/20/ 2020.
34. W. Bouamra, C. Djeddi, B. Nini, M. Diaz, and I. Siddiqi, "Towards the design of an offline signature verifier based on a small number of genuine samples for training," Expert Systems with Applications, vol. 107, pp. 182-195, 2018.
35. E. N. Zois, A. Alexandridis, and G. Economou, "Writer independent offline signature verification based on asymmetric pixel relations and unrelated training-testing datasets," Expert Systems with Applications, vol. 125, pp. 14-32, 2019.
36. S. N. Srihari, A. Xu, and M. K. Kalera, Learning strategies and classification methods for off-line signature verification, in: Int. Workshop on frontiers in Handwriting Recognit. 2004. pp. 161-166.
37. D. Rivard, E. Granger, and R. Sabourin, Multi-feature extraction and selection in writer-independent off-line signature verification, Int. J. Document Analysis and Recognit., 16 (2013), 83-103.
38. M. A. Ferrer, M. Diaz-Cabrera, and A. Morales, Static Signature Synthesis: A Neuromotor Inspired Approach for Biometrics, IEEE Trans. on Pattern Anal. and Machine Intell., 37 (2015), 667-680.
39. M. Diaz, M. A. Ferrer, G. S. Eskander, and R. Sabourin, "Generation of Duplicated Off-line Signature Images for Verification Systems," IEEE Trans. on Pattern Anal. and Machine Intell., 39 (2017), 951-964.
40. D. Bertolini, L. S. Oliveira, E. Justino, and R. Sabourin, Reducing forgeries in writer-independent off-line signature verification through ensemble of classifiers, Pattern Recognit., 43 (2010), 387-396.
41. E. Pękalska and R. P. W. Duin, Dissimilarity representations allow for building good classifiers, Pattern Recognit. Lett., 23 (2002) 943-956.
42. O. Tuzel, F. Porikli, P. Meer, Region Covariance: A Fast Descriptor for Detection and Classification, in: European Conf. Computer Vision, (ECCV) 2006, pp. 589-600.
43. Z. Gao, Y. Wu, M. Harandi, Y. Jia, A Robust Distance Measure for Similarity-Based Classification on the SPD Manifold, IEEE Trans. Neural Networks Learn. Systems, 31 (2020), 3230-3244.
44. P. Koniusz, L. Wang, and A. Cherian, Tensor Representations for Action Recognition, IEEE Trans. on Pattern Anal. and Machine Intell., 44 (2022), 648-665.

45. Cherian, S. Sra, Positive Definite Matrices: Symmetric positive definite (SPD) matrices Data Representation and Applications to Computer Vision, in: Algorithmic Advances in Riemannian Geometry and Applications. Advances in Computer Vision and Pattern Recognition., H. Q. Minh and V. Murino, Eds., Springer, Cham, 2016, pp. 93-114, doi: 10.1007/978-3-319-45026-1_4
46. P. Zanini, M. Congedo, C. Jutten, S. Said, Y. Berthoumieu, Transfer Learning: A Riemannian Geometry Framework With Applications to Brain–Computer Interfaces, IEEE Trans. Biomedical Engineering, 65 (2018) 1107-1116.
47. Edelman, T. A. Arias, S. T. Smith, The geometry of algorithms with orthogonality constraints, SIAM Journ. Matrix Anal. and Applications, 20 (1998), 303-353.
48. X. Pennec, Intrinsic Statistics on Riemannian Manifolds: Basic Tools for Geometric Measurements, J. of Math. Imag. Vis., 25, (2006) 127.
49. S. Said, L. Bombrun, Y. Berthoumieu, J. H. Manton, Riemannian Gaussian Distributions on the Space of Symmetric Positive Definite Matrices, IEEE Trans.Inf. Theory, 63 (2017) 2153-2170.
50. S. Jayasumana, R. Hartley, M. Salzmann, H. Li, M. Harandi, Kernel Methods on Riemannian Manifolds with Gaussian RBF Kernels, IEEE Trans. Pattern Anal. Mach. Intell., 37 (2015), 2464-2477.
51. X. Pennec, P. Fillard, and N. Ayache, A Riemannian Framework for Tensor Computing, Int. J. Comput. Vis. 66 (2006) 41–66.
52. C. Atkinson, A. F. S. Mitchell, Rao's Distance Measure, Sankhyā: The Indian Journal of Statistics, Series A (1961-2002), 43 (1981), 345-365.
53. N. J. Higham, Functions of matrices: Theory and computation, SIAM, 2008.
54. O. Tuzel, F. Porikli, P. Meer, Pedestrian Detection via Classification on Riemannian Manifolds, IEEE Trans. Pattern Anal. Mach. Intell., 30 (2008), 1713-1727.
55. R. Wang, H. Guo, L. S. Davis, Q. Dai, Covariance discriminative learning: A natural and efficient approach to image set classification, in Comput. Vis. Pattern Recognit. (CVPR), 2012, pp. 2496-2503.
56. S. Lai, L. Jin, Y. Zhu, Z. Li, and L. Lin, SynSig2Vec: Forgery-Free Learning of Dynamic Signature Representations by Sigma Lognormal-Based Synthesis and 1D CNN, IEEE Trans. on Pattern Anal. and Machine Intell., 44 (2022), 6472-6485.
57. M. M. Yapıcı, A. Tekerek, N. Topaloğlu, Deep learning-based data augmentation method and signature verification system for offline handwritten signature, Pattern Anal. Appl., 24 (2021), 165-179.
58. V. Ruiz, I. Linares, Ã. Sãnchez, J. F. Vẽlez, Off-line Signature Verification using Compositional Synthetic Generation of Signatures and Siamese Neural Networks, Neurocomputing, 374 (2019) 30-41.
59. M. Diaz-Cabrera, M. A. Ferrer, A. Morales, Cognitive Inspired Model to Generate Duplicated Static Signature Images, in: Int. Conf. Front. Handwriting Recognit. (ICFHR), 2014, pp. 61-66.
60. G. Cheng, B. C. Vemuri, A Novel Dynamic System in the Space of SPD Matrices with Applications to Appearance Tracking, SIAM J. on Imaging Sc., 6 (2013) 592-615.
61. M. Moakher, A Differential Geometric Approach to the Geometric Mean of Symmetric Positive-Definite Matrices, SIAM J. on Matrix Anal. and Appl., 26 (2005), 735-747.
62. B. Afsari, Riemannian L^p center of mass: Existence, uniqueness, and convexity, Proc. of the American Math. Soc. 139 (2011), 655-673.
63. P. Zanini, M. Congedo, C. Jutten, S. Said, Y. Berthoumieu, Parameters estimate of Riemannian Gaussian distribution in the manifold of covariance matrices, in: IEEE Sensor Array and Multichannel Signal Processing Workshop (SAM), 2016, doi: 10.1109/SAM.2016.7569687
64. M. K. Kalera, S. Srihari, A. Xu, Offline signature ve rification and identification using distance statistics, Int. Journ. of Pattern Recognit. and Artif. Intel., 18 (2004) 1339-1360.

65. S. Pal, A. Alaei, U. Pal, and M. Blumenstein, Performance of an Off-Line Signature Verification Method Based on Texture Features on a Large Indic-Script Signature Dataset, in: IAPR (DAS), (2016), 72-77.
66. Alaei, S. Pal, U. Pal, and M. Blumenstein, An Efficient Signature Verification Method Based on an Interval Symbolic Representation and a Fuzzy Similarity Measure, IEEE Trans. on Inform. Forensics and Secur. 12 (2017), 2360-2372.
67. F. Leclerc and R. Plamondon, Automatic Signature Verification: The State Of The Art: 1989–1993, Int. J. of Pattern Recognit. and Artificial Intel. 8(1994), 643-660.
68. R. Tolosana, R. Vera-Rodriguez, C. Gonzalez-Garcia, J. Fierrez, A. Morales, J. Ortega-Garcia, et al., SVC-onGoing: Signature verification competition, Pattern Recognit. 127, (2022), 108609.
69. P. R. Prajapati, S. Poudel, M. Baduwal, S. Burlakoti, S. P. Panday, Signature Verification using Convolutional Neural Network and Autoencoder, J. of the Inst. of Eng., 16 (2021) 33-40.
70. K. Bhunia, A. Alaei, P. P. Roy, Signature verification approach using fusion of hybrid texture features, Neural Comput. Appl. 31 (2019), 8737-8748.
71. M. Diaz, M. A. Ferrer, and R. Sabourin, Approaching the intra-class variability in multi-script static signature evaluation, in: (ICPR), 2016, pp. 1147-1152.